Dual-Level Direct Dynamics Study on the Diels−Alder Reaction of Ethylene and 1,3-Butadiene

Chun-Huei Huang, Li-Chao Tsai, and Wei-Ping Hu*

Department of Chemistry, National Chung Cheng University, Chia-Yi, Taiwan 621

Received: July 16, 2001; In Final Form: August 30, 2001

Dual-level direct dynamics study was performed on the forward and reverse reaction of the parent Diels−Alder reaction of ethylene and 1,3-butadiene. The underlying potential energy surface was mapped with HF/6-31G* theory while the correlated methods including MP2/6-31+G* and QCISD(T)/6-31+G* were used to build a more accurate description of the reaction path necessary for the dual-level variational transition state theory calculation including multidimensional tunneling. By modeling the experimental gas-phase rate constants, our calculation estimated a forward classical barrier height of 21.9 kcal/mol, which is significantly lower than that inferred from the experimental activation energy (27.5 kcal/mol). The reverse barrier height is estimated as 69.6 kcal/mol, giving a classical energy of reaction of −47.8 kcal/mol, in good agreement with available experimental values. The variational effects were found to be negligible in this reaction, and the tunneling effects were small except at lower temperature. The deuterium and ^{13}C kinetic isotope effects (KIEs) of the forward reaction were also calculated and were consistent with available experimental data in related systems. Both the vibrational and rotational motions were found to contribute strongly to the inverse secondary deuterium KIEs, and the tunneling effects make a noticeable contribution to the normal primary ^{13}C KIEs at low temperature.

Introduction

The Diels−Alder reaction is one of the most important types of reaction in organic synthesis. Its mechanisms, energetics, and transition state properties have been extensively studied in the past decades.[1−13] It is now generally accepted that the reaction of ethylene and 1,3-butadiene, the parent Diels−Alder reaction,

$$C_2H_4 + C_4H_6 \rightarrow C_6H_{10} \qquad \text{(Rxn 1)}$$

proceeds via a synchronous[6,11] concerted pathway. However, the value of the classical energy barrier (classical energy is also called Born−Oppenheimer energy, which is the sum of the electronic energy and the nuclear repulsion energy) of this pathway, despite of many theoretical studies over the years, has not been accurately established. Most of the recent theoretical calculation using complete active space self-consistent field (CASSCF),[7,8,14] Møller−Plesset perturbation theory (MP),[6,11,13,15,16] density functional theory (DFT),[10,11,13,17] and configuration interaction (CI)[7,8,13,18] methods predicted values that ranged from 18 to 44 kcal/mol, and it seemed that the dynamics correlation is very important for the calculation.[7−9,11,13] The experimental activation energy at high temperature (487−648 °C) is 27.5 ± 2 kcal/mol.[1] However, it is well-known that the activation energy includes zero-point energy and various thermal effects, and it can be different from the classical barrier height by several kcal/mol. In contrast to the extensive theoretical study of the stationary points (reactants, products, and transition states), there is relatively little high-level modeling of the reaction dynamics for the parent Diels−Alder reaction. Most of the dynamics calculation applied conventional transition state theory (TST),[19,20] and the possible tunneling effects were estimated using simple one-dimensional tunneling approximation.[8−13] The dynamical aspects of variational effects (the shifting of the reaction bottleneck from the saddle point)[20,21] and multidimensional tunneling,[20−24] which are important in many cases,[20,21,25−29] have not been explored. Furthermore, the kinetic isotope effect (KIE) has long been used as a sensitive tool to probe the reaction mechanisms of many organic reactions. The roles variational and multidimensional tunneling effects play in the KIE of this reaction are also unknown.

Accurate modeling of the polyatomic reacting system taking into account the variational and tunneling effects is difficult because it requires accurate global information of the potential energy surface (PES). Traditionally, the PES information is obtained through a fitted analytical function or is calculated using semiempirical electronic structure theory. However, a global analytical surface is very difficult to build and the dynamics results are sometimes sensitive to the functional forms employed. Semiempirical calculation is very efficient for obtaining global PES information, but its accuracy is often questionable, especially at points far from stable geometry on the PES. Advances in the recent years on the computer technology and interfacing between the electronic structure and the dynamics calculation have made accurate modeling of important organic reactions using accurate ab initio methods possible. In the current study, we applied the recently developed dual-level dynamics approach[30−32] to model the reaction rate constants of the parent Diels−Alder reaction with variational transition state theory including multidimensional tunneling (VTST/MT)[20−24] calculation. The dual-level dynamics method was developed to handle large chemical systems without sacrificing too much of the accuracy. In the method,[30] a qualitatively correct level of theory (the low level) is chosen to evaluate the underlying potential energy surface information, and a more accurate level (the high level) of theory is used to

* Corresponding author. E-mail: chewph@ccunix.ccu.edu.tw. Fax: 886-5-272-1040.

10.1021/jp012740f CCC: $20.00
Published on Web 10/06/2001

calculate the most important stationary point information pertinent to the reaction. Interpolated correction is then applied to correct the low-level PES based on the high-level data. The dual-level VTST/MT methods have been shown to be able to accurately model the thermal rate constants of a variety of chemical reactions over extended temperature range.[30−36] Recently, we have also developed a set of new interpolated correction schemes (the SIL schemes)[29,36] for the dual-level VTST/MT calculation. These schemes include an intermediate-level calculation to better estimate the reaction barrier width and thus the tunneling effects. In the current study, we first obtain an estimate of the forward and reverse classical barrier heights of the parent Diels−Alder reaction (the concerted pathway) by modeling the experimental forward and reverse rate constants using dual-level VTST/MT calculation with the SIL-2 correction scheme.[29] We then calculate the reaction rate constants of the isotopically substituted reactions:

$$C_2D_4 + C_4H_6 \rightarrow C_6H_6D_4 \qquad \text{(Rxn 2)}$$

$$C_2H_4 + C_4D_6 \rightarrow C_6H_4D_6 \qquad \text{(Rxn 3)}$$

$$^{13}C_2H_4 + {}^{13}C_4D_6 \rightarrow {}^{13}C_6H_4D_6 \qquad \text{(Rxn 4)}$$

All four reactions have the same classical barrier heights within Born−Oppenheimer approximation. The kinetic isotope effects (KIEs) due to the above three types of substitutions are then evaluated and analyzed.

Methods

Molecular geometry and relative energies of the reactant, product, and transition state were obtained using the Hartree−Fock method[15,18] with the 6-31G* basis set[37] and Møller−Plesset second-order perturbation theory[15,16] with the 6-31G* and 6-31+G* basis sets. Counterpoise (CP)[38,39] correction has also been applied to the MP2/6-31+G* results. The classical barrier height and energy of reaction were also calculated with the quadratic configuration interaction theory[40,41] including single and double substitutions (QCISD) and with the triples contribution added pertubatively [QCISD(T)] with the 6-31+G* basis set at the geometry obtained at the HF/6-31G* and MP2/6-31+G* levels. Dual-level VTST/MT calculation was performed to model the forward and reverse rate constants of Rxn 1. The canonical variation theory (CVT),[20,21] where a single reaction bottleneck is located for a given temperature, was used to calculate the variational effects. The microcanonical multidimensional tunneling (μOMT)[22,24] approach, which takes the dominant tunneling probability calculated by the small- and large-curvature approximations (SCT[23] and LCT[21,22]) at every energy grid, was used to estimate the tunneling correction. In the dual-level VTST/MT calculation, the low-level (LL) theory, which was used to map the underlying potential energy surface information, was HF/6-31G*, and the high-level (HL) geometry and frequency information on the stationary points was obtained using MP2/6-31+G* theory. In the low-level calculation, the reaction path was calculated from −3.5 bohrs on the reactant side to 3.0 bohrs on the product side using the Page−McIver[42] algorithm with the gradient and hessian steps of 0.005 and 0.05 bohrs, respectively, and the reduced mass was set to 1 amu. The reaction coordinate of the product is estimated to be 4.64 bohrs by extrapolating the C−C bond length along the reaction path. The redundant internal coordinates[43] were used for vibrational analysis on the reaction path. The intermediate level calculation that was used to estimate the high-level barrier width was at the QCISD(T)/6-31+G* level using the reaction-path geometry calculated by the low-level theory. The SIL-2[29] correction scheme was then applied to determine the range parameters to make the corrected vibrationally adiabatic ground-state potential (V_a^G, which is the sum of the classical energy on the minimum energy path, V_{MEP}, and the vibrational zero-point energy) curve consistent with the estimated barrier width.

A misunderstanding usually caused in the application of SIL schemes is that the "apparent" level of theory used in the intermediate-level calculation is "higher" than that of the high-level calculation. As has been discussed in previous work,[30,36] the high-level data here mean the results from the highest-level geometry optimization and vibrational frequency calculation along with the estimated barrier height. The purpose of intermediate-level calculation is to estimate the barrier width using an affordable high-accuracy energy calculation along the low-level reaction path. It does not necessarily mean that the theory used in the intermediate-level energy calculation should be a "lower" level of theory than what is applied in the high-level geometry optimization/frequency calculation. Thus, in the current study, the intermediate level calculation, QCISD(T)/6-31+G*, was carried out to obtain a reliable estimation of the barrier width to be used in the dual-level calculation while the MP2/6-31+G* results formed the highest available geometry and frequency data at the stationary points. Furthermore, since the high-level barrier height was determined by fitting to the experimental data, conceptually it is thus a "higher" level of energy calculation than the intermediate level.

The original SIL-2 scheme was developed for a bimolecular reaction with two reactant and two product molecules. Here we made a straightforward extension of the SIL-2 scheme to the reaction with a single product molecule. The reactant-side half-height width ($s_{1/2}$, or more appropriately in the current study, $s_{1/2,R}$) is still determined by the intermediate level calculation, as described in the original SIL-2 scheme.[29] When there is only one product molecule, the dual-level interpolated correction[30] requires different functional forms and a range parameter (B_P, as defined in ref 30) for the correction functions on the product side. We first define the product-side half-height width ($s_{1/2,P}$) as the product-side reaction coordinate on which the classical energy is the same as that on $s_{1/2,R}$

$$V_{MEP,HL}(s_{1/2,P}) = V_{MEP,HL}(s_{1/2,R}) = {}^1/_2\Delta V^{\ddagger}_{HL} \qquad (1)$$

where $\Delta V^{\ddagger}$ is the forward classical barrier height. The $s_{1/2,P}$ is estimated the same way as $s_{1/2,R}$ using the intermediate level calculation. We then estimate the high-level vibrational zero-point energy (ZPE) of the generalized transition state (GT) at $s_{1/2,P}$ as

$$ZPE^{GT}{}_{HL}(s_{1/2,P}) = ZPE^{GT}{}_{LL}(s_{1/2,P}) + (ZPE^{\ddagger}{}_{HL} - ZPE^{\ddagger}{}_{LL}) + \delta \qquad (2)$$

$$\delta = [{}^1/_2\Delta V^{\ddagger}{}_{HL}/(\Delta V^{\ddagger}{}_{HL} - \Delta E_{rxn,HL})] \times \Delta \qquad (3)$$

$$\Delta = (ZPE^{P}{}_{HL} - ZPE^{P}{}_{LL}) - (ZPE^{\ddagger}{}_{HL} - ZPE^{\ddagger}{}_{LL}) \qquad (4)$$

where $ZPE^{\ddagger}$ is the vibrational zero-point energy of the transition state and ΔE_{rxn} is the classical energy of reaction. That is, we approximate the high-level ZPE at $s_{1/2,P}$ as the sum of the low-level ZPE plus a correction term that is interpolated linearly between the corrections at the transition state and the product. When applying the dual-level correction in a VTST/MT calculation, one can simultaneously adjust the range parameters

TABLE 1: Calculated Bond Lengths (Å) at Various Theoretical Levels

	C_2H_4	C_4H_6	C_6H_{10}	TS
R1				
MP2/6-31+G* [a]			1.529	2.279
MP2/6-31G* [b]			1.529	2.285
B3LYP/6-31G[c]			1.537	2.273
HF/6-31G* [d]			1.531	2.202
CASSCF/6-31G* [e]				2.223
R2				
MP2/6-31+G*		1.459	1.346	1.412
MP2/6-31G*		1.458	1.342	1.414
B3LYP/6-31G		1.457	1.337	1.407
HF/6-31G*		1.458	1.321	1.393
CASSCF/6-31G*		1.465		1.397
R3				
MP2/6-31+G*		1.348	1.506	1.384
MP2/6-31G*		1.344	1.505	1.380
B3LYP/6-31G		1.341	1.510	1.383
HF/6-31G*		1.343	1.500	1.377
CASSCF/6-31G*		1.342		1.398
R4[f]				
MP2/6-31+G*	1.340		1.528	1.387
MP2/6-31G*	1.336		1.527	1.382
B3LYP/6-31G	1.331		1.535	1.386
HF/6-31G*	1.317		1.520	1.383
CASSCF/6-31G*	1.338			1.400

[a] This work. [b] This work. [c] Reference 11. [d] This work. [e] Reference 7. [f] Experimental C−C bond length = 1.337 Å, ref 55.

L and B_P such that the corrected V_a^G values agree with the high-level classical energy values ($^1/_2\Delta V^{\ddagger}_{HL}$) plus the estimated ZPE values at the reaction coordinates $s_{1/2,R}$ and $s_{1/2,P}$, respectively. In the current study, the forward and reverse barriers were adjusted separately to reproduce the experimental rate constants, and thus the high-level energy of the reaction is set to the difference of the estimated classical barriers (forward−reverse). Harmonic approximation was used for all vibrational modes since no low-frequency hindered-rotor mode is present. The ICL[44] scheme was used for the frequency correction, and the linear method[29,30] was used for the energy correction in the nonadibatic region in the LCT calculation. The forward and reverse reaction symmetry numbers (from the rotational partition functions) were set to 8 and 2, respectively.

In the current study, the electronic structure calculation was performed using the Gaussian 98 program,[37] and the dual-level direct dynamics calculation was carried out using a locally modified Gaussrate 8.2 program,[45] which provides an interface between the Gaussian 98 and the Polyrate 8.2[46] VTST/MT program. The above calculation was performed on several PC workstations running Red Hat Linux and on an Origin 2000 sever in the National Center for High-Performance Computing in Taiwan.

Results and Discussion

(1) Geometry and Energetics. Table 1 and Figure 1 show the calculated geometry of the reactants, transition state, and product at HF/6-31G*, MP2/6-31G*, and MP2/6-31+G* levels, Houk et al.'s B3LYP/6-31G* and CASSCF/6-31G* values are also included for comparison. Only the concerted singlet transition state is considered in the current study. At the MP2/6-31+G* level, the *s-cis* form of 1,3-butadiene is 2.5 kcal/mol higher in classical energy than the *s-trans* form, and the boat form of cyclohexene is 5.0 kcal/mol higher than the twisted form. Thus, as seen in Figure 1, the *s-trans*-1,3-butadiene and the twisted form of the cyclohexene are taken as the reactant and product, respectively. The HF/6-31G* method predicted

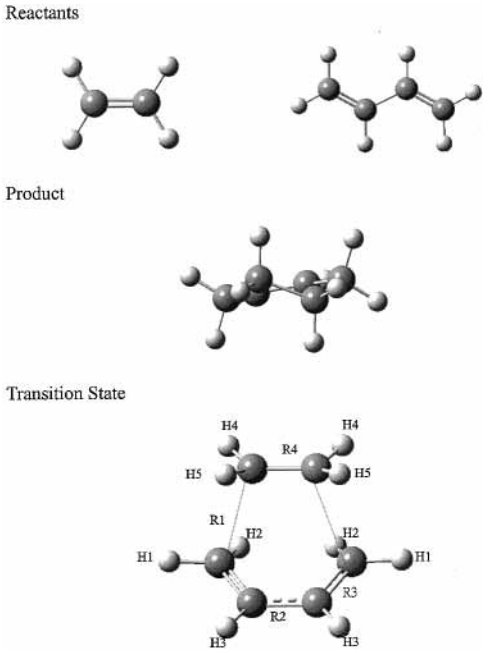

Figure 1. Geometry of the reactants, products, and transition state.

TABLE 2: Calculated Forward Reaction Energetics (Born−Oppenheimer Energies, kcal/mol)

method	$\Delta V^{\ddagger}$	$-\Delta E_{rxn}$
HF/6-31G*	45.0	42.9
MP2/6-31G*	17.9	52.5
CASSCF/6-31G*	43.8[a]	
QCISD(T)/6-31G*//CASSCF/6-31G*	22.5[a]	
BeckeLYP3/6-31G*	22.4[b]	43.1[b]
MP2/6-31+G*	18.5	48.8
MP2/6-31+G* with Cp[c]	23.5	
QCISD/6-31+G*//HF/6-31G*	31.0	43.8
QCISD/6-31+G*//MP2/6-31+G*	29.8	44.2
QCISD(T)/6-31+G*//HF/6-31+G*	27.1	43.0
QCISD(T)/6-31+G*//MP2/6-31+G*	25.9	43.1
Best fit[d]	21.9	47.8
Experiment	27.5 ± 2[e]	45.1[f]

[a] From ref 7. [b] From ref 11. [c] Counterpoise correction. [d] By fitting to the experimental rate constants; see text. [e] From the experimental activation energy in ref 1, not directly comparable to other values in the table; see text for discussion. [f] From ref 47 and zero-point and thermal energies calculated at MP2/6-31+G* level.

shorter C−C bond lengths in the transition state than those by the MP2 calculation, especially for R1 (∼0.08 Å shorter). The calculated MP2/6-31G* and MP2/6-31+G* C−C bond lengths are very similar (within 0.01 Å) and they are also very close to the B3LYP/6-31G* results by Houk et al.[11] Table 2 lists the calculated and experimental reaction energetics. The experimental[47] enthalpy of reaction is −40.0 kcal/mol at 298 K, which translates to the Born−Oppenheimer (classical) energy of reaction of −45.1 kcal/mol using the zero-point and thermal energies obtained at the MP2/6-31+G* level. Most of the calculated energies of reaction in Table 2 are in reasonable agreement with the experimental value. It is noted that the inclusion of the carbon diffuse function makes the MP2/6-31+G* calculation agree better with the experiment. The calculated forward barrier heights range from 18 (MP2/6-31G*) to 45 kcal/mol (HF/6-31G*). As compared to the HF/6-31G* results, the CASSCF calculation gives only slightly longer bond lengths and very similar barrier heights. This suggests a single determinant is a reasonable first approximation to the electronic wave function. Calculations that include dynamic electron

correlation (MP2, B3LYP, QCISD, etc.) lower the barrier significantly (>10 kcal/mol). The forward activation energy derived from Rowley and Steiner's[1] experimental data is 27.5 kcal/mol. However, the experimental activation energy includes various thermal contributions and is usually several kcal/mol different from the classical energy barrier on the Born−Oppenheimer potential energy surface. The reverse reaction activation energy was obtained by Uchiyama et al.[2] to be 66.2 kcal/mol. Combining the two barriers, one obtains an estimated energy of reaction of −38.7 kcal/mol, which is consistent with the experimental enthalpy of reaction mentioned above. In the current study, we took the forward and reverse classical energy barriers as adjustable parameters, and they were adjusted to minimize the root-mean-square (RMS) differences between the experimental and theoretical (CVT/μOMT) rate constants. As will be discussed later in this section, our best estimate for the forward and reverse classical barriers are 21.9 and 69.6 kcal/mol, respectively. This leads to a classical reaction energy of −47.8 kcal/mol, in good agreement with the derived experimental energy of reaction mentioned above. The estimated forward barrier is very close to Houk et al.'s[11] B3LYP/6-31G* value and the MP2/6-31+G* value with counterpoise calculation, and, to a lesser extent, to the results of QCISD(T) calculation. Table 2 also suggests that the MP2 energies should be used with caution in this type of reaction since the counterpoise correction is large (5 kcal/mol). The apparent difference between the activation energy and the classical barrier height, and the difference between the enthalpy and the classical energy of reaction is partly due to the difference in the vibrational zero-point energies. In Rxn 1, the ZPE of the reactants, transition state, and the product calculated at MP2/6-31+G* level are 86.3, 88.7, and 93.6 kcal/mol, respectively.

From Table 2, it seems that the B3LYP method could also be used as the low-level theory in the dual-level dynamics calculation. Unfortunately, the estimated cost of the frequency calculation, which has to be carried out hundreds of times in the calculation, is 3−4 times that of a corresponding Hartree−Fock calculation. In addition, although it is encouraging that the barrier predicted by the B3LYP/6-31G* level is within 1 kcal/mol from that of the estimated "true" value, as discussed previously,[36] this makes the energy correction in the region between the reactant and transition state difficult. That is, if the B3LYP method predicts an incorrect barrier width, it cannot be easily corrected in the dual-level calculation. The use of DFT methods with nonlocal correlation functionals as the low-level calculation could be further investigated in the future.

(2) Rate Constants. By minimizing the RMS differences between the calculated (CVT/μOMT) and experimental (forward and reverse) rate constants of Rxn 1 at high temperatures, as shown in Figures 2 and 3, we obtained the estimated forward and reverse classical energy barriers of 21.85 and 69.60 kcal/mol, respectively. The calculated rate constants using the above estimated barriers are listed in Tables 3 and 4. Calculation using the Wigner tunneling formula was also included for comparison. We found that the variational effects are negligible in the current system, as shown in Tables 3 and 4 since the TST and CVT values are almost identical. Figure 4 shows the calculated dual-level classical and vibrationally adiabatic ground-state energy curves (V_{MEP} and V_a^G) along the reaction path of Rxn 1. Clearly, the reaction is dominated by the central barrier; that is, the V_a^G curve peaks sharply at the transition state. The calculated forward TST and CVT/μOMT rate constants of Rxn 1 in the entire temperature range (200−1000 K) are plotted in Figure 5. As can be seen in the figure, there is almost no observable curvature in the Arrhenius plot in the entire temperature range except at very low temperature. In fact, from Table 3 we see

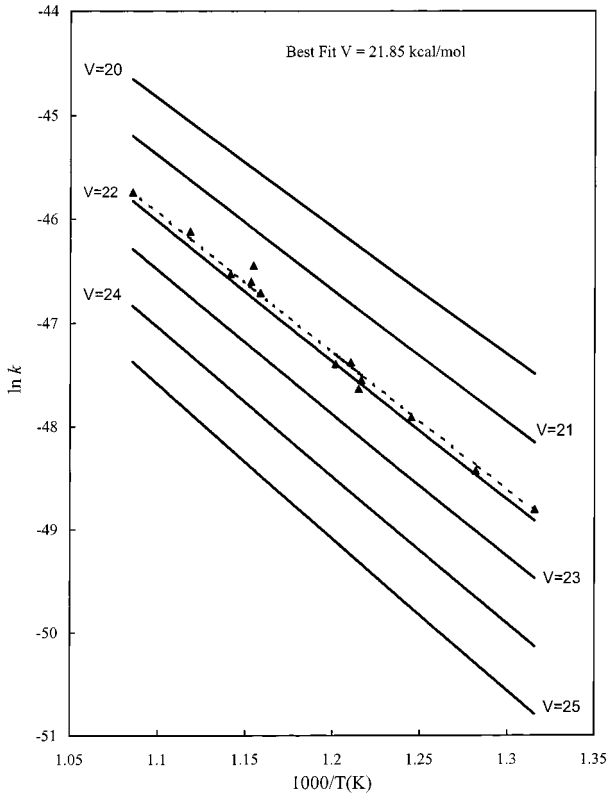

Figure 2. Modeling the experimental forward rate constants of Rxn 1 by adjusting the classical barrier height. The solid triangles are experimental rate constants by Rowley and Steiner in ref 1.

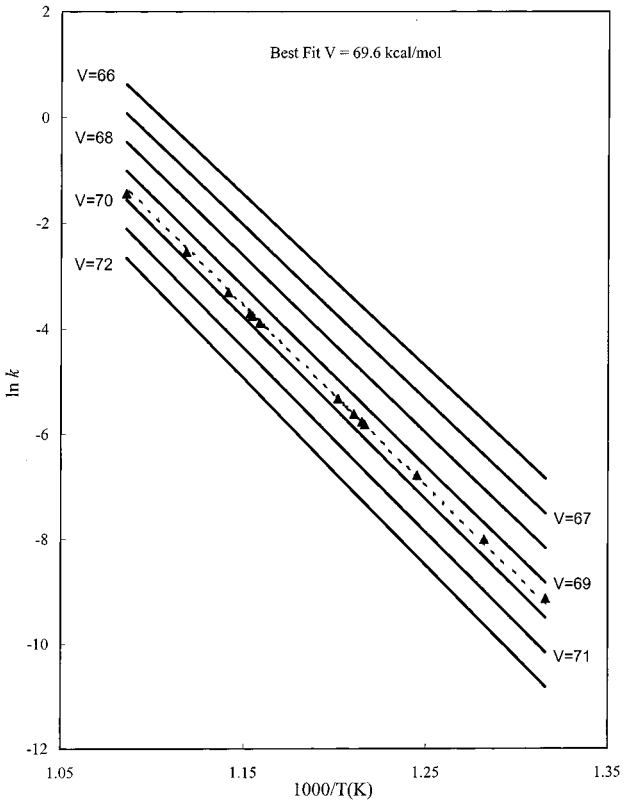

Figure 3. Modeling the experimental reverse rate constants of Rxn 1 by adjusting the classical barrier height. The solid triangles are from the experimental Arrhenius fit in ref 2c.

TABLE 3: Calculated Dual-Level Rate Constants (cm^3 $molecule^{-1}$ s^{-1}) for the Diels−Alder Reaction of $C_2H_4 + C_4H_6 \rightarrow C_6H_{10}$

T (K)	TST	CVT	TST/W[b]	CVT/μOMT	exp[c]
200	1.48(−41)[a]	1.41(−41)	2.31(−41)	4.73(−41)	
250	2.41(−36)	2.41(−36)	3.27(−36)	4.72(−36)	
300	7.44(−33)	7.43(−33)	9.27(−33)	1.16(−32)	
400	1.88(−28)	1.88(−28)	2.14(−28)	2.39(−28)	
500	9.18(−26)	9.18(−26)	9.99(−26)	1.07(−25)	
600	6.19(−24)	6.19(−24)	6.57(−24)	6.87(−24)	
760	5.89(−22)	5.89(−22)	6.11(−22)	6.28(−22)	6.15(−22)
800	1.41(−21)	1.41(−21)	1.46(−21)	1.49(−21)	1.53(−21)
850	3.78(−21)	3.78(−21)	3.90(−21)	3.98(−21)	4.23(−21)
900	9.18(−21)	9.18(−20)	9.43(−21)	9.60(−21)	1.05(−20)
921	1.30(−20)	1.30(−20)	1.33(−20)	1.35(−20)	1.48(−20)
1000	4.25(−20)	4.25(−20)	4.34(−20)	4.40(−20)	

[a] 1.48(−41) means 1.48×10^{-41}. [b] TST with the Wigner tunneling correction. [c] Calculated from the experimental Arrhenius fit[1] (760 to ~921 K) 3.0×10^{10} exp(−27500/RT) cm^3 $molecule^{-1}$ s^{-1}.

TABLE 4: Calculated Dual-Level Rate Constant (s^{-1}) for the Retro-Diels−Alder Reaction of $C_6H_{10} \rightarrow C_2H_4 + C_4H_6$

T (K)	TST	CVT	TST/W	CVT/μOMT	exp[a]
200	3.22(−58)	3.21(−58)	5.01(−58)	1.06(−57)	
250	7.00(−44)	6.99(−44)	9.49(−44)	1.40(−43)	
300	2.79(−34)	2.79(−34)	3.48(−34)	4.41(−34)	
400	3.35(−22)	3.35(−22)	3.82(−22)	4.29(−22)	
500	6.87(−15)	6.87(−15)	7.48(−15)	8.02(−15)	
600	5.60(−10)	5.60(−10)	5.94(−10)	6.23(−10)	
800	8.69(−4)	8.69(−4)	8.99(−4)	9.22(−4)	9.64(−4)
900	1.04(−1)	1.04(−1)	1.07(−1)	1.09(−1)	1.01(−1)
1000	4.83	4.83	4.94	5.01	4.14

[a] Calculated from the experimental Arrhenius fit[2c] $\log k = 15.15 - 66560/4.58T$ or $k = 3.8 \times 10^6$ exp(−28877/RT) s^{-1}.

that the μOMT tunneling correction increases the forward CVT rate constant by 6% at 800 K and by 56% at 300 K. The tunneling correction for the reverse reaction is similar, as seen in Table 4, increasing the CVT rate by 6% and 58% at 800 and 300 K, respectively. Although the tunneling is almost negligible at higher temperatures, it is nonetheless significant at lower temperatures. In comparison with some of the earlier studies on hydrogen abstraction reactions,[27,30,31,34,48] the tunneling contribution to the rate constants in the current system is not particularly large, considering the large barrier of the this reaction. However, this is as expected since the reaction path corresponds primarily to the motion of the relatively heavy carbon atoms in the current system. The small curvature tunneling is found to be the dominant tunneling mechanism. Similar behaviors were found in the calculated dual-level rate constants of Rxn 2, Rxn 3, and Rxn 4 that are included in the Supporting Information. It is noted that, within the Born−Oppenheimer approximation, all the isotopically substituted reactions have the same classical barrier heights, and thus the estimated barriers for Rxn 1 mentioned above were used in the dual-level VTST/MT calculation for Rxn 2−Rxn 4. As also seen in Tables 3 and 4, the popular Wigner tunneling correction[21] predicted smaller tunneling correction at all temperatures than the μOMT method. For example, at 300 K the Wigner correction increases the TST rate constant of the forward reaction by 25%, as compared to the 56% by the μOMT method. Since the Wigner correction is only valid when the tunneling energies are very close to the top of the barrier whose shape resembles an inverted parabola, and when there is little reaction-path curvature, it is thus not always a reliable tunneling correction method. However, in the current study, the Wigner correction is not totally out of line because the tunneling effects are not very large and the most important tunneling energies are near the top of the barrier. In contrast, the multidimensional tunneling correction methods (SCT and LCT) used in the current study take the entire reaction path or swath information into consideration, and they have been

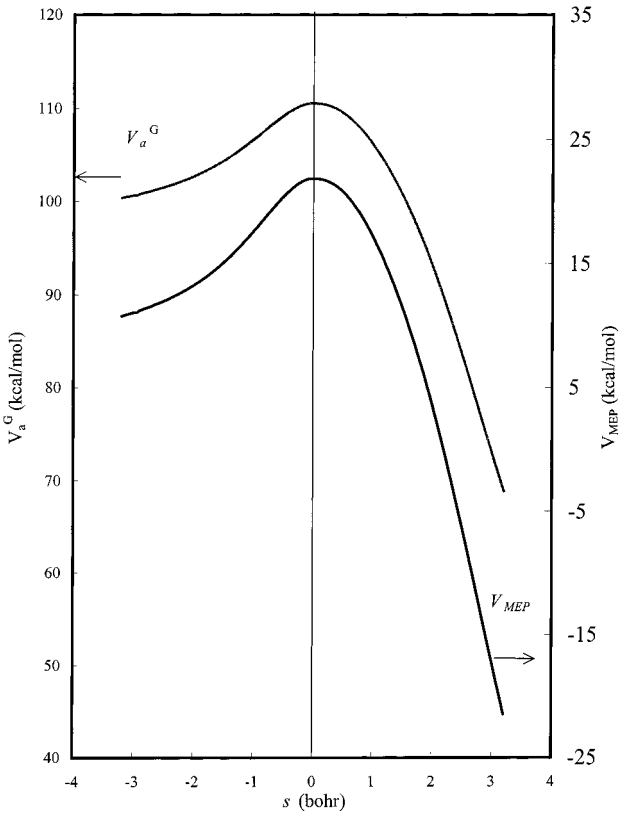

Figure 4. Calculated dual-level potential energy curves of Rxn 1 along the reaction path.

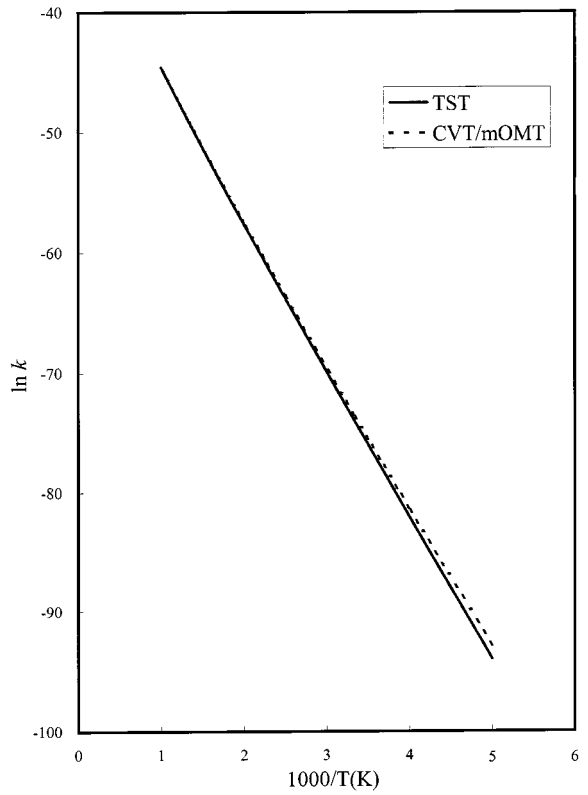

Figure 5. Arrhenius plot of the calculated dual-level rate constants of Rxn 1 over the entire temperature range.

TABLE 5: Calculated KIE1 (k_{Rxn1}/k_{Rxn2}) by TST and CVT/μOMT Theory

T (K)	TST	CVT/μOMT
200	0.748	0.838
250	0.837	0.891
300	0.892	0.928
400	0.947	0.968
500	0.972	0.986
600	0.985	0.995
800	0.996	1.004
1000	1.000	1.008

TABLE 6: Calculated KIE2 (k_{Rxn1}/k_{Rxn3}) by TST and CVT/μOMT Theory

T (K)	TST	CVT/μOMT
200	0.629	0.718
250	0.723	0.776
300	0.787	0.824
400	0.865	0.887
500	0.908	0.923
600	0.934	0.945
800	0.962	0.970
1000	0.977	0.982

tested against accurate quantum scattering results[20] and have been able to reproduce experimental rate constants and kinetic isotope effects in both low-[27,30,31,34,48] and high-barrier systems.[22,23a,25]

One may be concerned that the overestimation of the vibrational frequencies and thus the zero-point energies by the low- and high-level calculation could cause additional uncertainty on the estimated barrier heights. Although the overestimation by the Hartree−Fock method is well-known, the frequencies used in the dual-level dynamics calculation have already been corrected to the corresponding high-level (MP2/6-31+G*) values. The possible errors caused by the current treatment of the vibrational motion are assessed as follows. The usually used frequency/ZPE scaling factors for the MP2/6-31G* method is 0.94−0.97,[49] although whether these factors are suitable for transition states is *unclear*. If we take 0.94 as a global scaling factor and assume that the major uncertainty caused by the vibrational treatment is from the ZPE values, then since for Rxn 1 the ZPE of the transition state is 2.4 kcal/mol higher than that of the reactants at the high level, the approximate error in the ZPE difference is 0.14 kcal/mol. Similarly, the ZPE of the product is 4.9 kcal/mol higher than that of the transition states, the approximate error is 0.29 kcal/mol. As a result, due to the uncertainty in the vibrational treatment the obtained forward classical barrier (21.85 kcal/mol) might be underestimated by 0.14 kcal/mol and the reverse classical barrier (69.60 kcal/mol) might be overestimated by 0.29 kcal/mol.

(3) Kinetic Isotope Effects. The kinetic isotope effect (KIE) is defined here by the ratio of the bimolecular rate constant of Rxn 1 to the rate constant of isotopically substituted reactions Rxn 2, Rxn 3, and Rxn 4.

$$\mathrm{KIE1} = k_{\mathrm{Rxn1}}/k_{\mathrm{Rxn2}} \tag{5}$$

$$\mathrm{KIE2} = k_{\mathrm{Rxn1}}/k_{\mathrm{Rxn3}} \tag{6}$$

$$\mathrm{KIE3} = k_{\mathrm{Rxn1}}/k_{\mathrm{Rxn4}} \tag{7}$$

The KIE1 and KIE2 are secondary deuterium isotope effects while KIE3 is the primary ^{13}C isotope effect. The calculated KIEs by TST and CVT/μOMT as a function of temperature are shown in Tables 5−7 and in Figure 6. Both KIE1 and KIE2 are inverse (less than unity) at most temperatures and show slight positive temperature dependence. At 300 K, the calculated CVT/μOMT KIE1 and KIE2 are 0.928 and 0.824, respectively. As shown in the tables, KIEs calculated by CVT/μOMT are slightly larger than those calculated by TST. At 300 K, the inclusion of tunneling increased the calculated KIE1 and KIE2 by 4% and 5%, respectively. In contrast to KIE1 and KIE2, KIE3 is normal (greater than unity) and is 1.187 by CVT/μOMT at 300 K, 10% higher than the TST value. The slightly inverse KIE1 and KIE2 and slightly normal KIE3 are consistent with the available experimental data on the Diels−Alder reactions of substituted dienes and dienophiles.[3,8−12] It is usually instructive to factorize the calculated KIEs to contributions from translational, rotational, and vibrational motions, and from variational and tunneling effects,[31,33,35,36,50]

TABLE 7: Calculated KIE3 (k_{Rxn1}/k_{Rxn4}) by TST and CVT/μOMT Theory

T (K)	TST	CVT/μOMT
200	1.083	1.428
250	1.079	1.258
300	1.075	1.187
400	1.068	1.125
500	1.062	1.097
600	1.057	1.082
800	1.051	1.065
1000	1.048	1.057

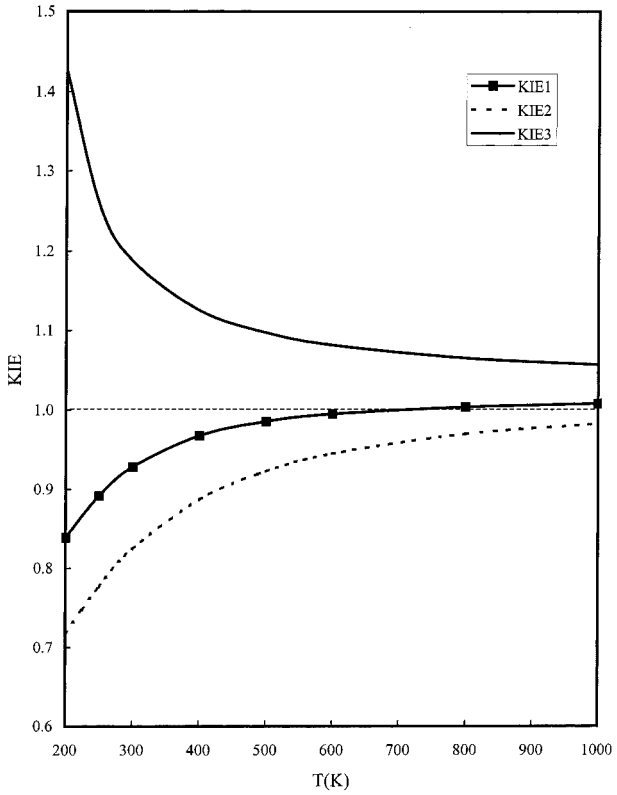

Figure 6. Temperature dependence of the calculated KIEs.

$$\mathrm{KIE} = \eta_{\mathrm{trans}}\eta^{\ddagger}_{\mathrm{rot}}\eta^{\ddagger}_{\mathrm{vib}}\eta_{\mathrm{var}}\eta_{\mathrm{tunneling}} \tag{8}$$

where the ‡ sign signifies that the rotational and vibrational contributions are evaluated at the transition state. The various contributions to KIE1, KIE2, and KIE3 are listed in Tables 8−10. As shown in Tables 8 and 9, the small secondary KIEs actually result from the balance between the inverse vibrational contribution and normal rotational contribution. The inverse vibrational contribution is mainly due to the increase of ZPE

TABLE 8: Factor[a] Analysis of KIE1

T (K)	$\eta_{\text{vibrational}}$	$\eta_{\text{variational}}$	$\eta_{\text{tunneling}}$
200	0.378	1.001	1.121
250	0.423	1.001	1.065
300	0.451	1.001	1.042
400	0.479	1.000	1.022
500	0.492	1.000	1.014
600	0.499	0.999	1.010
800	0.506	0.999	1.006
1000	0.508	0.999	1.005

[a] The translational and rotational contributions are independent of temperature, and they are 1.138 and 1.737, respectively.

TABLE 9: Factor[a] Analysis of KIE2

T (K)	$\eta_{\text{vibrational}}$	$\eta_{\text{variational}}$	$\eta_{\text{tunneling}}$
200	0.456	1.001	1.142
250	0.524	1.001	1.075
300	0.571	1.001	1.048
400	0.628	1.000	1.025
500	0.660	1.000	1.016
600	0.679	0.999	1.011
800	0.700	0.999	1.006
1000	0.711	0.999	1.005

[a] The translational and rotational contributions are independent of temperature, and they are 1.054 and 1.308, respectively.

TABLE 10: Factor[a] Analysis of KIE3

T (K)	$\eta_{\text{vibrational}}$	$\eta_{\text{variational}}$	$\eta_{\text{tunneling}}$
200	0.945	0.999	1.319
250	0.942	0.999	1.161
300	0.938	0.999	1.105
400	0.931	1.000	1.054
500	0.926	1.000	1.034
600	0.922	1.000	1.023
800	0.917	1.000	1.013
1000	0.914	1.000	1.008

[a] The translational and rotational contributions are independent of temperature, and they are 1.111 and 1.032, respectively.

from the reactant to the transition state. The KIE2 is more inverse than KIE1 not because of more inverse vibrational contribution as one might guess, but it is actually due to the smaller rotational contribution. Most of the temperature dependence of the KIE1 and KIE2 is from the vibrational contributions. The variational contribution, as mentioned above, is totally negligible, and the tunneling effects make a slightly normal contribution to the KIEs. The vibrational contribution to KIE3 is only slightly inverse because the mass difference ($^{12}C/^{13}C$) is relatively small. The normal KIE3 is due to the normal translational, rotational, and the tunneling contributions that are 1.111, 1.032, and 1.105 at 300 K, respectively. Interestingly, the inverse vibrational contribution of KIE3 shows slightly negative temperature dependence. This is because the ZPE differences in Rxn 1 and Rxn 4 are very small and thus the entropy effects dominate the temperature dependence of the ratios of the vibrational partition functions. While the variational contribution is still negligible, the tunneling contribution to normal KIE3 is noticeable at low temperatures. As seen in Table 10, tunneling also contributes to the temperature dependence of KIE3.

As seen in Tables 5−7, most of the calculated KIEs using TST and CVT/μOMT are not very different. However, since the KIE study is usually used as a very sensitive tool to determine from the competing reaction mechanisms or pathways, small differences may sometimes be important. Furthermore, the current Diels−Alder reaction is a somewhat lucky case that the KIEs can be modeled reasonably by conventional transition state theory. This is because the variational effects are very small due to the large classical barrier, and the tunneling is not very important because the reaction path motion is dominated by the movement of heavy atoms. In organic reactions with relatively high barriers (>5 kcal/mol) where hydrogen atoms are transferred, the tunneling effects may contribute significantly to KIEs, and the multidimensional tunneling correction has to be applied. For low-barrier reactions, the zero-point or the entropy effects may cause significant variational effects, which can in turn make important contribution to KIEs.

(4) Single Reaction Path KIEs. Despite their importance in elucidating reaction mechanisms, most KIEs have only been modeled by the conventional transition state theory. The variational contribution was usually ignored and the tunneling contribution was only roughly estimated. Recently, dual-level VTST/MT calculations have been performed on a few systems to model the temperature dependence of KIEs and their various contributions.[25−27,30,31,33−36,50,51] Most of the calculations were, however, based on semiempirical or analytical PES, and full ab initio direct dynamics KIE study is rare.[36] The difficulty lies in the fact that to obtain accurate PES information to perform a VTST/MT calculation for the unsubstituted reaction is hard enough already, the significant additional computational cost for calculating the substituted PES usually makes accurate ab initio direct dynamics KIE study impractical. The KIE study by TST does not have this limitation since all the necessary information is based on equilibrium structures (stationary points on PES). Truhlar et al. have recently developed a very cost-effective method to calculate the KIEs by VTST/MT using information from a single reaction path.[52] This method is based on polynomial expansion of the PES around the reaction path and on the reorientation of the optimized dividing surface (RODS)[52−54] algorithm. In the current study we have tested the single-reaction-path KIE method against the directly calculated KIE1, KIE2, and KIE3 discussed earlier this section using dual-level direct dynamics method. We found that at 300 K the calculated KIEs by the two methods were within 1%. Thus, it seems that for most practical purposes, the KIEs can be modeled quite accurately by the single-reaction-path method. The expensive recalculation of the substituted reaction paths seems unnecessary for the current system. We then used this single-reaction-path method to calculate the KIEs by substituting the five different types of hydrogen atoms (see Figure 1 for labeling) in the transition state with deuterium atoms, as studied previously by Houk et al.[11] The calculated KIEs by the CVT/μOMT method at 298.15 and 373.15 K are compared with Houk et al.'s B3LYP values in Table 11. The corresponding experimental values[12] of a similar system are also included. The various contributions to the calculated KIEs are factorized in Table 12. As seen in Table 11, the two studies predicted very similar secondary deuterium kinetic isotope effects, and they are in good agreement with the available experimental data. The H2 KIEs are mostly inverse not solely because of the vibrational contribution but also due to the smallest normal rotational contribution, as seen in Table 12. The vibrational contributions to the H4 and H5 KIEs are mostly inverse; however, their rotational contributions are also the highest because the hydrogen atoms reside on a very small reactant molecule. As a result, the H4 and H5 KIEs are slightly higher than H2 KIEs. There are almost no changes in the hybridization on H3 from the reactant to the transition state, and the small inverse vibrational contribution and the small normal rotational contribution almost cancel

TABLE 11: Calculated KIEs at Different Levels of Theory at 298.15 and 373.15 K

	298.15 K				373.15 K		
	TST[a]	CVT/μOMT[b]	TST-B3LYP[c]	exp[d]	TST	CVT/μOMT	TST-B3LYP
H1=D	0.936	0.974	0.97	0.956, 0.968	0.961	0.984	0.98
H2=D	0.856	0.907	0.92	0.908, 0.938	0.899	0.931	0.94
H3=D	0.980	1.029	1.00	0.990	0.985	1.015	1.00
H4=D	0.897	0.946	0.94		0.932	0.962	0.96
H5=D	0.918	0.964	0.95		0.945	0.974	0.97

[a] Current work, using MP2/6-31+G** geometry and frequencies. [b] Current work using dual-level VTST/MT, see text. [c] Houk et al.'s B3LYP results in ref 11. [d] Experimental values for reaction of isoprene with maleic anhydride, taken from ref 11.

TABLE 12: Factor Analysis of the Calculated CVT/μOMT KIEs

	298.15 K		373.15 K			
	$\eta^{\ddagger}_{vib}$	η_{tun}	$\eta^{\ddagger}_{vib}$	η_{tun}	$\eta^{\ddagger}_{rot}$[a]	η_{trans}[a]
H1	0.803	1.038	0.825	1.023	1.139	1.019
H2	0.727	1.093	0.767	1.059	1.097	1.019
H3	0.866	1.050	0.871	1.030	1.110	1.019
H4	0.611	1.055	0.635	1.033	1.371	1.070
H5	0.632	1.050	0.651	1.030	1.358	1.070

[a] The rotational and translational contributions are independent of temperature.

out each other, resulting KIEs are very close to unity. As also seen in Table 12, tunneling effects increase the KIEs by 4−9% at 298.15 K and thus are not totally negligible. For many chemical reactions, the normal rotational contribution (and to a lesser extent, the translational contribution) to the secondary deuterium KIEs tends to cancel out the inverse vibrational contribution, and this results in only slightly inverse secondary KIEs. In contrast, for primary deuterium KIEs, all three contributions are normal, and large KIEs are usually observed at or below room temperature. The tunneling contribution is usually normal for high-barrier reactions but it may become slightly inverse for reactions with very low barriers.[35,36]

Summary

We have performed the first full ab initio dual-level VTST/MT study on the parent Diels−Alder reaction between ethylene and 1,3-butadiene. The forward and reverse classical barrier heights estimated from the current dynamics modeling are 21.9 and 69.6 kcal/mol, respectively. (The errors caused by the incomplete treatment of the vibrational motion in the current study are estimated to be a few tenths of 1 kcal/mol) These values could be used to calibrate the performance of various theoretical methods in calculating the reaction barrier heights. The variational effects are found to be negligible in the reaction, while the tunneling effects become significant at low temperature. Three isotopically substituted forward reactions (Rxn 2−Rxn 4) were also studied, and the KIEs were calculated. The slightly inverse secondary deuterium KIEs are caused primarily by the balance of the inverse vibrational contribution and the normal rotational contribution. The slightly normal primary ^{13}C KIEs are caused by the slightly inverse vibrational contribution and the slightly normal translational and rotational contributions. Tunneling also makes noticeable normal contribution to the ^{13}C KIEs at low temperature. In the current study we extended the SIL-2 correction scheme to the unimolecular side of the reaction in a dual-level dynamics calculation. We also found that the KIEs can be modeled very accurately by using a single reaction path without the costly recalculation of the substituted reaction path. While it is somewhat comforting that the traditional way of modeling KIEs using conventional transition state theory and greatly simplified one-dimensional tunneling models agrees reasonably well with the more sophisticated dual-level VTST/MT calculation, the current study demonstrated that accurate modeling of the reaction rate constants and kinetic isotope effects of complex chemical systems using full ab initio dual-level VTST/MT *is* now feasible. The approach employed in the current study should be much more accurate than the conventional methods in modeling reactions where tunneling effects and/or variational effects are important. This theoretical technique is anticipated to be very useful in elucidating more insights into the dynamical behaviors of many different types of organic reactions.

Acknowledgment. This research is supported in part by the National Science Council of Taiwan, grant number NSC 89-2113-M-194-006. We thank Prof. Donald G. Truhlar of the University of Minnesota for providing the Gaussrate interface program. We are also grateful to the National Center for High-Performance Computing of Taiwan for providing the computational resources and technical support.

Supporting Information Available: Tables of calculated geometry, vibrational frequencies, rate constants, and parameters used in the SIL-2 scheme and a figure illustrating the determination of the reaction coordinate of the product. This material is available free of charge via the Internet at http://pubs.acs.org.

References and Notes

(1) Rowley, D.; Steiner, H. *Discuss. Faraday Soc.* **1951**, *10*, 198.
(2) (a) Uchiyama, M.; Tomioka, T.; Amano, A. *J. Phys. Chem.* **1964**, *68*, 1878. (b) Tsang W. *J. Chem. Phys.* **1965**, *42*, 1805. (c) Lewis, D. K.; Bergmann, J.; Manjoney, R.; Paddock, R. *J. Phys. Chem.* **1984**, *88*, 4112.
(3) Sauer, J. *Angew. Chem., Int. Ed. Engl.* **1967**, *6*, 16.
(4) Loncharich, R. J.; Houk, K. N. *Annu. Rew. Phys. Chem.* **1988**, *39*, 213 and references therein.
(5) Benardi, F.; Bottni, A.; Field, M. J.; Guest, M. F.; Hillier, I. H.; Robb, M. A.; Venturini, A. *J. Am. Chem. Soc.* **1988**, *110*, 3050.
(6) Houk, K. N.; Li, Y.; Evanseck, J. D. *Angew. Chem., Int. Ed. Engl.* **1992**, *31*, 682.
(7) Li, Y.; Houk, K. N. *J. Am. Chem. Soc.* **1993**, *115*, 7478.
(8) Houk, K. N.; Li, Y.; Storer, J.; Raimondi, L.; Beno, B. *J. Chem. Soc., Faraday Trans.* **1994**, *90*, 1599.
(9) Houk, K. N.; Gonzalez, J.; Li, Y. *Acc. Chem. Res.* **1995**, *28*, 81 and references therein.
(10) Wiest, O.; Houck, K. N.; Black; Thomas, B., IV. *J. Am. Chem. Soc.* **1995**, *117*, 8594.
(11) Goldstein, E.; Beno, B.; Houk, K. N. *J. Am. Chem. Soc.* **1996**, *118*, 6036.
(12) (a) Beno, B. R.; Houk, K. N.; Singleton, D. A. *J. Am. Chem. Soc.* **1996**, *118*, 9984. (b) Singleton, D. A., Thomas, A. A. *J. Am. Chem. Soc.* **1995**, *117*, 9357.
(13) Wiest, O.; Montiel, D. C.; Houk, K. N. *J. Phys. Chem. A* **1997**, *101*, 8378 and references therein.
(14) (a) Roos, B. O. *Adv. Chem. Phys.* **1987**, *69*, 339. (b) Roos, B. O. *Int. J. Quantum Chem. Symp.* **1980**, *14*, 175.
(15) Hehre, W. J.; Radom, L.; Schleyer, P. v. R.; Pople, J. A. *Ab initio Molecular Orbital Theory*; John Wiley & Sons: New York, 1986.
(16) Mϕller, C.; Plesset, M. S. *Phys. Rev.* **1934**, *46*, 616.
(17) Hohenberg, P.; Kohn, W. *Phys. Rev.* **1964**, *136*, B864.
(18) (a) Szabo, A.; Ostlund, N. S. *Modern Quantum Chemistry*; McGraw-Hill: New York, 1989; see also references therein (b) Foresman,

J. B.; Frisch, A. *Exploring Chemistry with Electronic Structure Methods*, 2nd ed.; Gaussian Inc.: Pittsburgh, 1996.

(19) Eyring, H. *J. Chem. Phys.* **1935**, *3*, 105.

(20) Truhlar, D. G.; Garrett, B. C. *Acc. Chem. Res.* **1980**, *13*, 440.

(21) Truhlar, D. G.; Isaacson, A. D.; Garrett, B. C. In *Theory of Chemical Reaction Dynamics*; Baer M., Ed.; CRC Press: Boca Raton, FL, 1985; Vol. 4, p 65.

(22) Liu, Y.-P.; Lu, D.-H.; Gonzalez-Lafont, A.; Truhlar, D. G.; Garrett, B. C. *J. Am. Chem. Soc.* **1993**, *115*, 7806.

(23) (a) Liu, Y.-P.; Lynch, G. C.; Truong, T. N.; Lu, D.-H.; Truhlar, D. G.; Garrett, B. C. *J. Am. Chem. Soc.* **1993**, *115*, 2408. (b) Lu, D.-h.; Truong, T. N.; Melissas, V. S.; Lynch, G. C.; Liu, Y.-P.; Garrett, B. C.; Steckler, R.; Isaacson, A. D.; Rai, S. N.; Hancock, G. C.; Lauderdale, J. G.; Joseph, T.; Truhlar, D. G. *Comput. Phys. Commun.* **1992**, *71*, 235.

(24) Truong, T. N.; Lu, D.-h.; Lynch, G. C.; Liu, Y.-P.; Melissas, V. Lafont, A.; Rai, S. N.; Steckler, R.; Garrett, B. C.; Joseph, T.; Truhlar, D. G. *Comput. Phys. Commun.* **1993**, *75*, 143.

(25) Corchado, J. C.; Espinosa-García, J.; Roberto-Neto, O.; Chuang, Y.-Y.; Truhlar, D. G. *J. Phys. Chem. A* **1998**, *102*, 4899.

(26) Corchado, J. C.; Truhlar, D. G.; Espinosa-García, J. *J. Chem. Phys.* **2000**, *112*, 9375.

(27) Roberto-Neto, Orlando; Coitiño, E. L.; Truhlar, D. G. *J. Phys. Chem. A* **1998**, *102*, 4568.

(28) Kim, Y.; Corchado, J. C.; Villà, J.; Xing, J.; Truhlar, D. G. *J. Chem. Phys.* **2000**, *112*, 2718.

(29) Huang, C.-H.; You, R.-M.; Lian, P.-Y.; Hu, W.-P. *J. Phys. Chem. A* **2000**, *104*, 7200.

(30) Hu, W.-P.; Liu, Y.-P.; Truhlar, D. G., *J. Chem. Soc., Faraday Trans.* **1994**, *90*, 1715.

(31) Corchado, J. C.; Espinosa-Garcia, J.; Hu, W.-P.; Rossi, I.; Truhlar, D. G. *J. Phys. Chem.* **1995**, *99*, 687.

(32) Chuang, Y.-Y.; Truhlar, D. G. *J. Phys. Chem. A* **1997**, *101*, 3808.

(33) Hu, W.-P.; Truhlar, D. G. *J. Am. Chem. Soc.* **1996**, *118*, 860.

(34) Hu, W.-P.; Rossi, I.; Corchado, J. C.; Truhlar, D. G. *J. Phys. Chem. A* **1997**, *101*, 6911.

(35) Wu, Y.-R.; Hu, W.-P. *J. Am. Chem. Soc.* **1999**, *121*, 10168.

(36) Lien, P.-Y.; You, R.-M.; Hu, W.-P. *J. Phys. Chem. A* **2001**, *105*, 2391.

(37) Frisch, M. J.; Trucks, G. W.; Schlegel, H. B.; Scuseria, G. E.; Robb, M. A.; Cheeseman, J. R.; Zakrzewski, V. G.; Millam, M.; Daniels, A. D.; Kudin, K. N.; Strain, M. C.; Farkas, O.; Tomasi, J.; Barone, V.; Cossi, M.; Cammi, R.; Mennucci, B.; Pomelli, C.; Adamo, C.; Clifford, S.; Ochterski, J.; Petersson, G. A.; Ayala, P. Y.; Cui, Q.; Morokuma, K.; Malick, D. K.; Rabuck, A. D.; Raghavachari, K.; Foresman, J. B. Cioslowski, J.; Ortiz, J. V.; Baboul, A. G.; Stefanov, B. B.; Liu, G.; Liashenko, A.; Piskorz, P.; Komaromi, I.; Gomperts, R.; Martin, R. L.; Fox, D. J.; Keith, T.; Al-Laham, M. A.; Peng, C. Y.; Nanayakkara, A.; Gonzalez, C.; Challacombe, M.; Head-Gordon, M.; Replogle, E. S.; Pople, J. A.; *Gaussian 98*, Revision A.7; Gaussian, Inc.: Pittsburgh, PA, 1998.

(38) Morokuma, K.; Kitaura, K. In *Chemical Applications of Atomic and Molecular Electronic Potential*; Poltizer, P., Truhlar, D. G., Eds.; Plenum: New York, 1981; p 215.

(39) Boys, S. F.; Bernardi, *F. Mol. Phys.* **1970**, *13*, 440.

(40) Raghavachari, K.; Trucks, G. W.; Pople, J. A.; Head-Gordon, M. *Chem. Phys. Lett.* **1989**, *157*, 479.

(41) Pople, J. A.; Head-Gordon, M.; Raghavachari, K. *J. Chem. Phys.* **1987**, *87*, 5968.

(42) (a) Page, M.; McIver, J. W., Jr. *J. Chem. Phys.* **1988**, *88*, 922. (b) Page, M.; Doubleday, C.; McIver, J. W., Jr. *J. Chem. Phys.* **1990**, *93*, 5634.

(43) Chuang, Y.-Y.; Truhlar, D. G. *J. Phys. Chem. A* **1998**, *102*, 242.

(44) Chuang, Y.-Y.; Truhlar, D. G. *J. Phys. Chem. A* **1997**, *101*, 3808.

(45) Corchado, J. C.; Chuang. Y.-Y.; Coitino, E. L.; Truhlar, D. G. *Gaussrate*, version 8.2; University of Minnesota: Minneapolis, 1999.

(46) Chuang. Y.-Y.; Corchado, J. C.; Fast, P. L.; Villa, J.; Hu, W.-P.; Liu, Y.-P.; Lynch, G. C.; Nguyen, K. A.; Jackels, C. F.; Gu, M. Z.; Rossi, I.; Coitino, E. L.; Clayton, S.; Melissas, V. S.; Steckler. R.; Garrett, B. C.; Isaacson, A. D.; Truhlar, D. G. *Polyrate*, version 8.2; University of Minnesota: Minneapolis, 1999.

(47) CRC Handbook of Chemistry and Physics, 74th ed.; Lide, D. R., Eds. CRC Press: Boca Raton, FL, 1993.

(48) (a) Melissas, V. S.; Truhlar, D. G. *J. Chem. Phys.* **1993**, *99*, 1013. (b) Melissas, V. S.; Truhlar, D. G. *J. Chem. Phys.* **1993**, *99*, 3542. (c) Melissas, V. S.; Truhlar, D. G. *J. Phys. Chem. A* **1994**, *98*, 875.

(49) (a) Pople, J. A.; Scott, A. P.; Wong, M. W.; Radom, L. *Isr. J. Chem.* **1993**, *33*, 345. (b) Foresman, J. B.; Frisch, A. *Exploring Chemistry with Electronic Structure Methods*, 2nd ed.; Gaussian Inc.: Pittsburgh, PA, 1996.

(50) (a) Zhao, X. G.; Tucker, S. C.; Truhlar, D. G. *J. Am. Chem. Soc.* **1991**, *113*, 826. (b) Hu, W.-P.; Truhlar, D. G. *J. Am. Chem. Soc.* **1994**, *116*, 7797. (c) González-Lafond, A.; Truong, T. N.; Truhlar, D. G. *J. Phys. Chem.* **1991**, *95*, 4618.

(51) (a) Chuang, Y.-Y.; Radhakrishnan, M. L.; Fast, P. L.; Cramer, C. J.; Truhlar, D. G. *J. Phys. Chem. A* **1999**, *103*, 4893. (b) Villà, J.; Corchado, J. C.; González-Lafont, A.; Lluch, J. M.; Truhlar, D. G. *J. Phys. Chem. A* **1999**, *103*, 5061. (c) Masgrau, L.; González-Lafont, A.; Lluch, J. M *J. Chem. Phys.* **2001**, *114*, 2154.

(52) Fast, P. L.; Corchado, J. C.; Truhlar, D. G. *J. Chem. Phys*. **1998**, *109*, 6237.

(53) Fast, P. L.; Truhlar, D. G. *J. Chem. Phys*. **1998**, *109*, 3721.

(54) Corchado, J. C.; Coitiño, E. L.; Chuang, Y.-Y.; Fast. P. L.; Truhlar, D. G. *J. Phys. Chem. A* **1998**, *102*, 2424.

(55) Chase, M. W., Jr.; Davies, C. A.; Downey, J. R., Jr.; Frurip, D. J.; McDonald, R. A.; Syverud, A. N. *J. Phys. Chem. Ref. Data* **1985**, *14*, Suppl. 1.